Charge Transfer Evidence between Carbon Nanotubes and Encapsulated Conjugated Oligomers

ARTICLE *in* THE JOURNAL OF PHYSICAL CHEMISTRY C · MAY 2011

Impact Factor: 4.77 · DOI: 10.1021/jp1121678

THE JOURNAL OF PHYSICAL CHEMISTRY C

ARTICLE

pubs.acs.org/JPCC

Charge Transfer Evidence between Carbon Nanotubes and Encapsulated Conjugated Oligomers

L. Alvarez,*[,†,‡] Y. Almadori,[†,‡] R. Arenal,[§,∥] R. Babaa,[⊥,▽] T. Michel,[†,‡] R. Le Parc,[†,‡] J-L. Bantignies,[†,‡] B. Jousselme,[⊥] S. Palacin,[⊥] P. Hermet,[†,‡] and J.-L. Sauvajol[†,‡]

[†]Université Montpellier 2, and [‡]CNRS, Laboratoire Charles Coulomb UMR 5221, F-34095, Montpellier, France

[§]Laboratoire d'Etude des Microstructures, CNRS-ONERA, 92322 Chatillon, France

[∥]Laboratorio de microscopias avanzadas (LMA), Instituto de Nanociencia de Aragon (INA), U. Zaragoza, c/Mariano Esquillor s/n, 50018 Zaragoza, Spain

[⊥]CEA, IRAMIS, SPCSI, Laboratoire de Chimie des Surfaces et Interfaces, 91191 Gif-sur-Yvette Cedex, France

[▽]Chemical Engineering Department, University of Technology PETRONAS (UTP), Ipoh- Perak, Malaysia

ABSTRACT: A hybrid system consisting of quaterthiophene derivative inserted into carbon nanotubes is studied. Encapsulation efficiency of the conjugated oligomers in the hollow core of nanotubes is investigated by transmission electron microscopy and spatial-resolved electron energy loss spectroscopy. Infrared spectroscopy showed evidence of a significant positive charge transfer on the inserted oligothiophene. Raman spectra display different behaviors depending on the excitation energy and correlated to the quaterthiophene optical absorption energy. At high excitation wavelength (far from the oligomer resonance), radial breathing modes exhibit a significant upshift consistent with an encapsulation effect. At low excitation wavelength (close to the oligomer resonance), both the G-band shift and the low-frequency modes vanishing suggest a significant charge transfer between the quaterthiophene and the nanotubes.

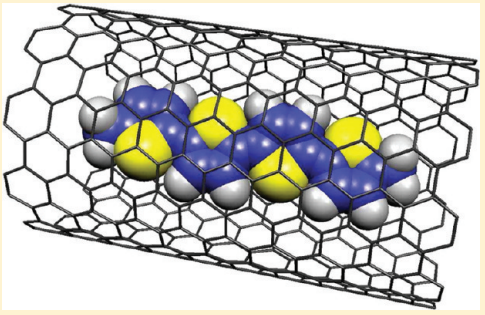

INTRODUCTION

Over the past few years, π-conjugated oligomers and polymers received considerable attention in the research community as they can play a crucial role in electronic and optoelectronic applications.[1−3] They are easy to manufacture at low cost and lightweight, making them very promising materials for devices for renewable and alternative energy sources.[4,5] They exhibit a great flexibility and are very light, allowing various ergonomics.[6,7] Thus, the organic materials display significant potential for competition with silicon in photovoltaic devices.[5] They, however, display some weak points like their brittleness and their low electric conductivity.[8] An efficient method to overcome those drawbacks consists of combining species with carbon nanotubes (NTs) to create a new hybrid system. Three methods are currently used for that purpose. The first one is a functionalization of polymers at the surface of the tubes.[9] This method has the advantage of producing strong interactions between the two species. On the other hand, it modifies the physical properties of the nanotubes by creating defects on its surface.[10] The second method is the noncovalent adsorption or wrapping of various functional molecules.[11] The third one consists of encapsulating oligomers inside nanotubes in order to keep their original physical properties.[8,12,13]

One of the most powerful tools to investigate carbon nanotube optical and electronic properties is Raman spectroscopy. Several spectral ranges in the Raman spectra of carbon nanotubes are of interest.[14,15] They are very sensitive to charge transfers and/or environmental effects, making it thus possible to investigate very efficiently the interaction between oligomer and nanotubes.

The first region of interest is located between 100 and 300 cm^{-1} where radial breathing modes (RBMs) related to the tube diameters are observed. The relationship between the frequency ω and the tube diameter d is usually given by the following equation: $\omega\ (cm^{-1}) = A/d\ (nm) + B$ where A and B are two constants.[14−16] Note that, under doping, a huge decrease or a loss of RBM intensity is observed.[17,18]

The second range, around 1600 cm^{-1}, exhibits the tangential modes (G-band). G-modes display different line shapes depending on the metallic or semiconducting character of the nanotubes.[14,15,19] Indeed, electron−phonon coupling (EPC) has been evidenced in carbon nanotubes,[20−23] and many works have demonstrated that G-modes are very sensitive to EPC.[23−26] Qualitatively, in semiconducting tubes, the profile of each G-band is narrow and symmetric. By contrast, bundles of metallic tubes display a broad low-frequency mode. The measurement of G-band gives therefore some insights into the metallic or

Received: December 22, 2010
Revised: April 28, 2011
Published: May 25, 2011

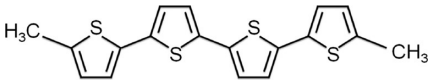

Figure 1. Structure of the 5,5‴-dimethyl-2,2′:5′,2″:5″,2‴-quaterthiophene, called for simplicity dimethyl-quaterthiophene (4T) in the text.

semiconducting character of nanotubes under investigations. Furthermore, Raman G-band has been shown to undergo a renormalization effect due to EPC[25] so that the phonon energy is reduced. Upon n or p doping, the strength of the EPC decreases, leading in both cases to an upshift of the G-band position.[25] One important point is that the magnitude of this shift depends on the tube diameter: the larger the diameter, the stronger the renormalization effect. On the other hand, a positive (respectively a negative) charging leads to a strengthening (respectively a softening) of the C−C bond and thus to an upshift (respectively a downshift) of the G-band.[26] Thus, for p type doping both effects shift the modes toward higher frequency. By contrast, a negative charging leads to a softening of the mode so that a competition between both effects takes place. Consequently, the direction of the G-band shift allows discriminating between n or p type doping of the nanotubes.[26] In particular, a downshift can only be assigned to a negative charging.

In this work, we study the properties of a hydrid system consisting of a 5,5‴-dimethyl-2,2′:5′,2″:5″,2‴-quaterthiophene (4T, Figure 1), trapped into carbon nanotubes. This material is called 4T@NT in the following of this article. Transmission electron microscopy (TEM) and spatial-resolved electron energy loss spectroscopy (SR-EELS) are used to investigate the morphology, the structure, and the chemical composition of the sample. The properties of 4T@NT, and especially the charge transfer between the oligomers and the nanotubes, are investigated by means of Raman and infrared (IR) spectroscopies.

EXPERIMENTAL SECTION

Sample Preparation. Two sources of nanotubes have been used: commercial electric arc single-walled carbon nanotubes, 90% purified (EA-NT in the following) provided from Nanocarblab[27] and CVD nanotubes (CVD-NT in the following) provided from Cheaptubes Company.[28]

Encapsulation of dimethyl-quaterthiophene (4T) into nanotubes (NTs) was performed using the vapor reaction method. Such method is similar to the one used for the elaboration of C_{60}-peapods.[29] Before the encapsulation treatment, carbon nanotubes were purified and open via thermal oxidation performed in air at 150 °C for 30 min. Then, NTs were mixed with 4T in weight ratio w_{CNT}/w_{4T} = 0.5, in a glass tube. The sample was outgased under 4.5×10^{-6} mbar at ambient temperature for 1 h followed by a thermal treatment at 100 °C for 3 h. Then, NTs with 4T were sealed in glass tube at 4.5×10^{-6} mbar and heated to 230 °C for 1 h. To remove 4T adsorbed on the outer walls of NTs, the sample was heated at 215 °C under 4.5×10^{-6} mbar for 1 h (sublimation temperature of 4T under 4.5×10^{-6} mbar is 210 °C). The sample was then washed with acetone and stored in the oven at 100 °C for 24 h.

Raman Spectroscopy. Raman experiments were performed on a triple monochromator spectrometer (Jobin Yvon T64000), equipped with a charge-coupled detector, in a back-scattering geometry, using the 458, 488, 568, 514.5, 647.1, and 752 nm excitation wavelengths. In order to avoid the heating of the tubes and oligomers, the laser power was adjusted at 700 μW with a spot diameter of about 3 μm using a 50× objective. The resolution is about 2 cm^{-1}.

Raman experiments with the 1064 nm excitation wavelength and photoluminescence spectra were measured using a Bruker RFS100 FT Raman spectrometer equipped with a nitrogen-cooled germanium detector. The excitation source is a continuous Nd:YAG laser emitting at 1.16 eV (1064 nm). Excitation at 1.16 eV allows the observation on the same spectra of the PL signal and the Stokes Raman signal (Raman shift in the range 100 and 3200 cm^{-1}. The resolution is about 4 cm^{-1}. For photoluminescence spectra, nanotubes have been dispersed in an aqueous solution with SDBS to obtain individual nanotubes.

Infrared Spectroscopy. Fourier transform infrared (FTIR) experiments were carried out on a Bruker IFS 66 V spectrometer equipped with a N2-cooled MCT (mercury cadmium telluride) detector. Transmission IR spectra were recorded in the 400−4000 cm^{-1} range. The spectral resolution was 2 cm^{-1}, and 64 scans were coadded for each spectrum.

TEM and SR-EELS. The TEM samples were prepared by dispersing the NTs powders in ethanol. The dispersions were ultrasonicated and subsequently deposited on a holey carbon 3 mm copper grid.

High-resolution TEM was performed using FEI Tecnai F20 and FEI CM20 microscopes both operating at 200 keV.

Spatial-resolved EEL spectra were recorded using a VG-HB501 dedicated scanning transmission electron microscope (STEM) instrument equipped with a cold field emission gun (FEG), operated at 100 keV with an energy resolution close to 0.7−0.8 eV in the core-loss region. Convergence angle on the sample and collection angle of the spectrometer were 15 and 24 mrad, respectively. This spectroscopic information was obtained using the spectrum-imaging (SPIM) acquisition mode.[30−33]

RESULTS AND DISCUSSION

TEM and SR-EELS studies were performed on 4T@CVD-NT. This sample contains both multiwalled (MWNT) and single-walled (SWNT) nanotubes. Figure 2a corresponds to an HR-TEM micrograph of 4T@NT sample. This micrograph clearly displays a double-walled nanotube filled with presumably 4T. This image is a very significant point. In fact, in the literature there are several examples showing similar HRTEM micrographs of filled NTs. However, as it is well-known in the field of electron microscopy, in NTs this conclusion might be an overinterpretation of the data because from this kind of HRTEM micrographs it is not possible to deduce the structure of this material, nor to obtain any chemical information. Thus, in order to go further in the analysis of these materials and to know where the 4T molecules are localized, we have developed SR-EELS. This technique is a very powerful tool to investigate such nanomaterials at the (sub)nanometer scale.[31]

First investigations concern individual NTs (Figure 2b, bright field (BF) image), acquiring a spectrum image (SPIM) in the whole area shown in the high-angle annular dark field (HAADF) image (Figure 2c). Figure 2d shows the intensity profiles of C and S extracted from the two chemical maps (C and S) obtained in the marked region of Figure 2c. From these intensity profiles, we can conclude that sulfur atoms are present inside the NTs. Thus, these profiles clearly demonstrate that sulfur atoms from the conjugated oligomers (4T) are mainly localized within few nanometers inside the NT, at its apex.

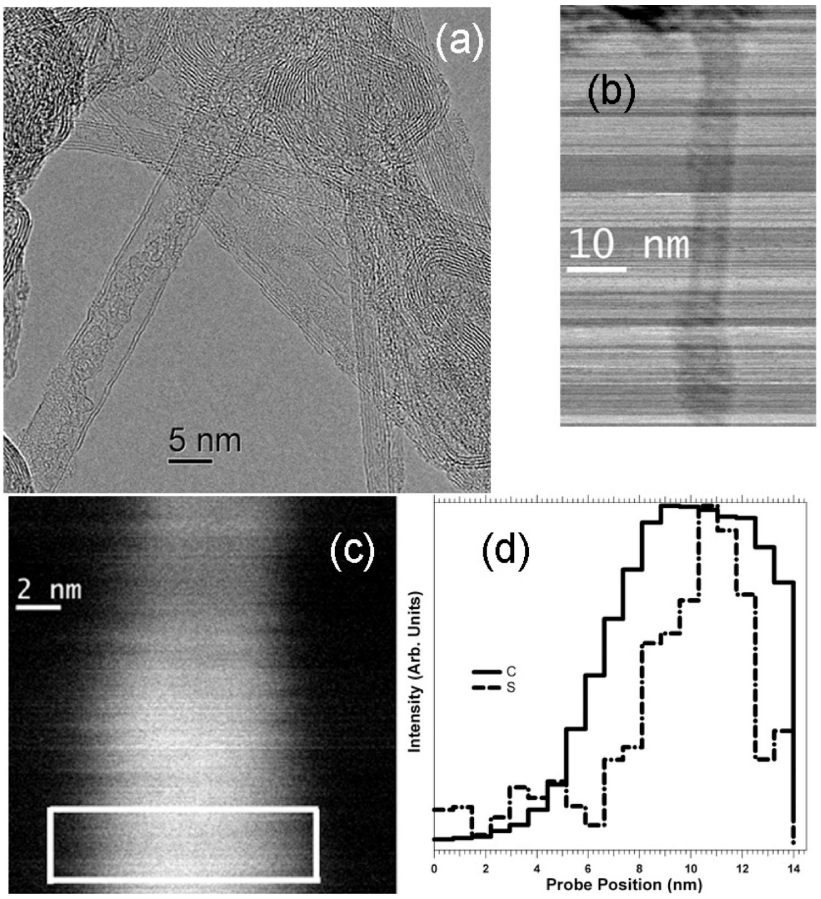

Figure 2. (a) HRTEM micrograph of a filled double-walled nanotube. (b) BF image of a MWNT. (c) HAADF image of this MWNT where a 24 × 24 SPIM has been recorded. (d) Intensity profile of C and S in the region marked in (b). These intensity profiles have been extracted from the C and S elemental maps that have been obtained from the analysis of the SPIM.

Structural and chemical properties of bundles of single-walled nanotubes have also been investigated (Figure 3). Figure 3a corresponds to an HAADF image acquired in parallel with the SPIM. Chemical maps of carbon and sulfur (Figures 3b and 3c) have been extracted from a 20 × 20 SPIM. Figure 3d shows two EEL spectra. Each of these two EEL spectra corresponds to the sum of 9 spectra (3 × 3 probe positions of the SPIM) recorded in the areas marked in Figure 3a. The energy loss near-edge feature (ELNES) of the C−K edge consisted of a π^* peak at ∼285 eV and a well-defined σ^* band starting at ∼292 eV.[30−34] The S−$L_{2,3}$ edge consist of a rather large peak around 165−220 eV. Carbon K edge at ∼284 eV is present in both of these two EEL spectra. These fingerprints are typical for the sp^2 hybridization of the C atoms in a graphitic network and indicate that the SWNTs are well crystallized. The $L_{2,3}$ edge of sulfur is clearly visible in Figure 3d(i). However, in the second EEL spectra of Figure 3d-(ii), the quantity of S (if any) is very low. This means that sulfur (from 4T) is not surrounding the bundles but mainly localized within the bundles, either inside the SWNT or in the interstitial sites in between three tubes. The sulfur chemical map confirms these results (Figure 3c). However, considering the 4T diameter (0.48 nm), the insertion into the free space (d = 0.40 nm for a tube diameter of 2 nm) in between three tubes is not likely and even impossible for smaller diameter tubes (for instance, the free space for a 1.5 nm tube diameter is 0.31 nm). We thus assume that 4T is localized in the hollow core of SWNTs. It is worth noting that the S distribution/repartition is rather uniform for the whole analyzed area of the bundle.

Figure 4 displays the photoluminescence spectra of aqueous solution of individual pristine CVD-NT and 4T@CVD-NT samples wrapped in SDBS recorded with an excitation wavelength of 1064 nm. The peak assignments of the different nanotubes have been derived from the work of S. Bachilo et al.[35] A clear red shift is observed between both samples. Such a red shift has been previously interpreted as an encapsulation effect of different molecules such as metallocenes[36] or squarylium dye,[37] inside carbon nanotubes. It is noteworthy that considering the 4T and the nanotube diameters (respectively 0.48 and 0.84 nm for the smallest (8,4) nanotube) and taking into account the van der Waals radius of a carbon nanotube wall (∼0.16 nm), all the nanotubes are expected to be filled and undergo the red shift as observed in Figure 4. This result is another insight into the efficiency of the encapsulation process.

Figure 5a displays the IR spectra of EA-NT, 4T, and 4T@EA-NT. The IR active modes of NTs are discussed elsewhere.[38,39] The expected IR absorption bands of the dimehyl-quaterthiophene are the following.[40−42] The bands at 1513 and 1445 cm^{-1} are associated respectively with the antisymmetric and the symmetric C═C stretching modes. The absorption band at 1279 cm^{-1} corresponds to antisymmetric in-plane C−H bending. The doublet at 1217 and 1166 cm^{-1} arises from the inter-ring C−C stretching vibration. The band at 1198 cm^{-1} can be

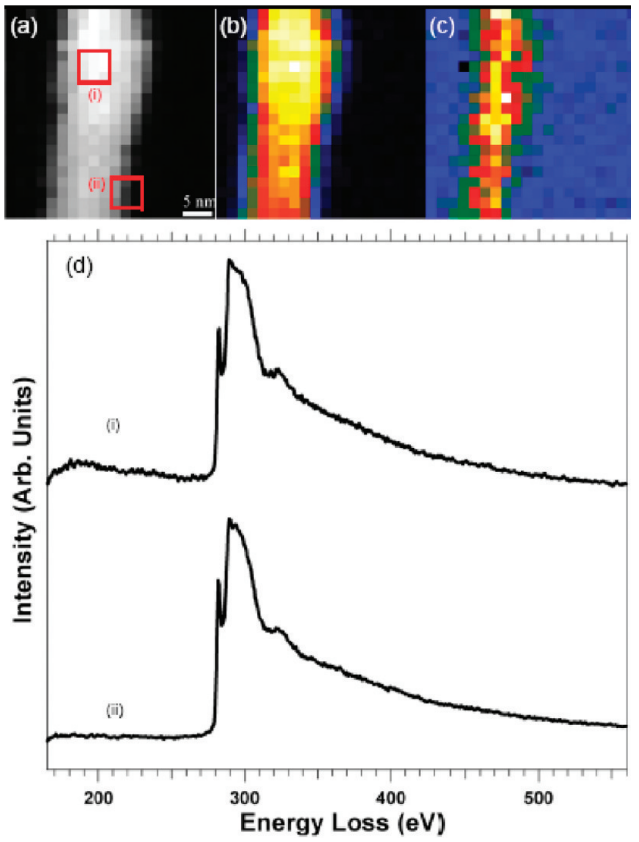

Figure 3. (a) HAADF image of a bundle of SWNTs on which we collected a 20 × 20 SPIM. (b) Carbon and (c) sulfur elemental maps, respectively, extracted from the SPIM. (d) Two spectra from the sum of 9 (3 × 3) EEL spectra extracted from the marked areas of (a). K edge of carbon (∼ 284 eV) ((i) and (ii)) and $L_{2,3}$ edge of sulfur (∼165−220 eV) only in (i).

probably related to antisymmetric stretching of the two-end $C_\alpha-CH_3$ bonds. Peaks at 1066 and 1042 cm^{-1} correspond to in-plane C−H bending. The multiplet of bands at 899 and 843 cm^{-1} arise from the symmetric and antisymmetric C−S stretching modes. The absorption bands at 795 and 787 cm^{-1} are assigned to the out-of-plane C−H bending vibrations. The weak band at 644 cm^{-1} is associated with an in-plane ring deformation mode.

The oligomer IR active modes and those of nanotubes are observed in the IR spectrum of the 4T@NT sample (Figure 5a). However, insertion into nanotubes clearly leads to significant modifications of the infrared modes of the oligomer, especially in the 600−900 and 1400−1600 cm^{-1} spectral ranges. Upon encapsulation, the intensity of some 4T modes significantly decreases and the frequency of the most intense band round 800 cm^{-1} is significantly downshifted and broadened. Figure 5b compares the IR spectra of 4T (circles, topmost) and 4T@EA-NT (triangles, bottommost) together with the IR spectra of raw and iodine-doped 4T (gray lines).[40] One can first check that the spectra corresponding to the pristine 4T measured in this work (circles) and in ref 40 (curve a) are quite similar. The iodine doping of 4T leads to the progressive vanishing of the main modes as a function of the doping level. The downward arrows indicate the peaks that are disappearing upon doping. Figure 5c details the IR spectra in the 950−600 cm^{-1} range of the pristine 4T and 4T inserted into EA-NT. The most intense band in 4T

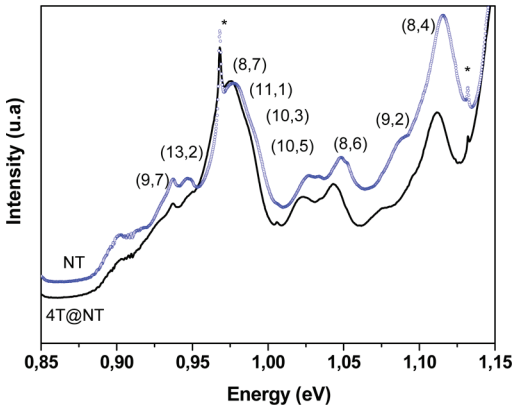

Figure 4. Superimposed Raman and photoluminescence spectra recorded at 1064 nm excitation wavelength of aqueous suspensions with SDBS of pristine NT (blue open circles) and 4T@NT(CVD) (black line) samples. Stars indicate the Raman modes of nanotubes.

contains three modes located at 786, 795, and 800 cm^{-1}. In the 4T@EA-NT sample, only a broad and downshifted single band is measured at 786 cm^{-1}. It must be pointed out that the same behavior is found in iodine-doped 4T (see Figure 5b (curve d) and Table 1 of ref 40). For instance, a peak around 670 cm^{-1} which appears on iodine-doped 4T is observable in Figure 5c.

In summary, we found out a lot of similarities between the IR spectra of 4T inserted into NT and iodine-doped 4T. Iodine is well-known to be an electron acceptor leading to a positive charging 4T in iodine-doped 4T sample. The similarities between the IR spectrum of 4T@NT and I@4T sample state that 4T oligomers undergo a significant positive charge transfer when they are trapped inside nanotubes.

To confirm this assumption, we performed Raman spectroscopy to investigate carbon nanotubes behavior after 4T encapsulation. The Raman spectrum of the 4T excited at 647.1 nm gives rise to several modes in the 600−1600 cm^{-1} spectral range (Figure 6, bottom). The main features are the following: weak lines at 1564, 1533, and 1503 cm^{-1} probably related to C═C vibrations localized at the two outer thiophene rings; 1482 (its shoulder at 1469) and 1448 cm^{-1} peaks assigned to C═C stretching modes; the 1261 and 1224 cm^{-1} lines associated with inter-ring C−C stretching modes; the 1165 cm^{-1} contribution assigned to outer-ring C−C bond; the 1058 and 1044 cm^{-1} lines corresponding to in-plane C−H deformation; the 736 and 694 cm^{-1} peaks related to C−S stretching modes.[40,41] It must be emphasized that a huge photoluminescence signal prevents the study of the 4T vibrations in the Raman spectrum excited at 514.5 nm (2.41 eV).

The Raman spectrum of 4T@NT excited at 647.1 and 514.5 nm are displayed in Figure 6. Vibrations of the trapped oligomers are observed in both spectra. It must be pointed out that the huge photoluminescence which prevents the measurement of the 4T Raman spectrum at 514.5 nm is bleached when 4T molecules are inserted into nanotubes (Figure 6, top) making the oligomer Raman features observable at this excitation wavelength with a relative strong intensity (Figure 6, top spectrum). The photoluminescence bleaching is another hint of a significant interaction between 4T and the nanotubes. Furthermore, this quenching also suggests that the amount of free oligomer molecules within our samples is completely negligible.

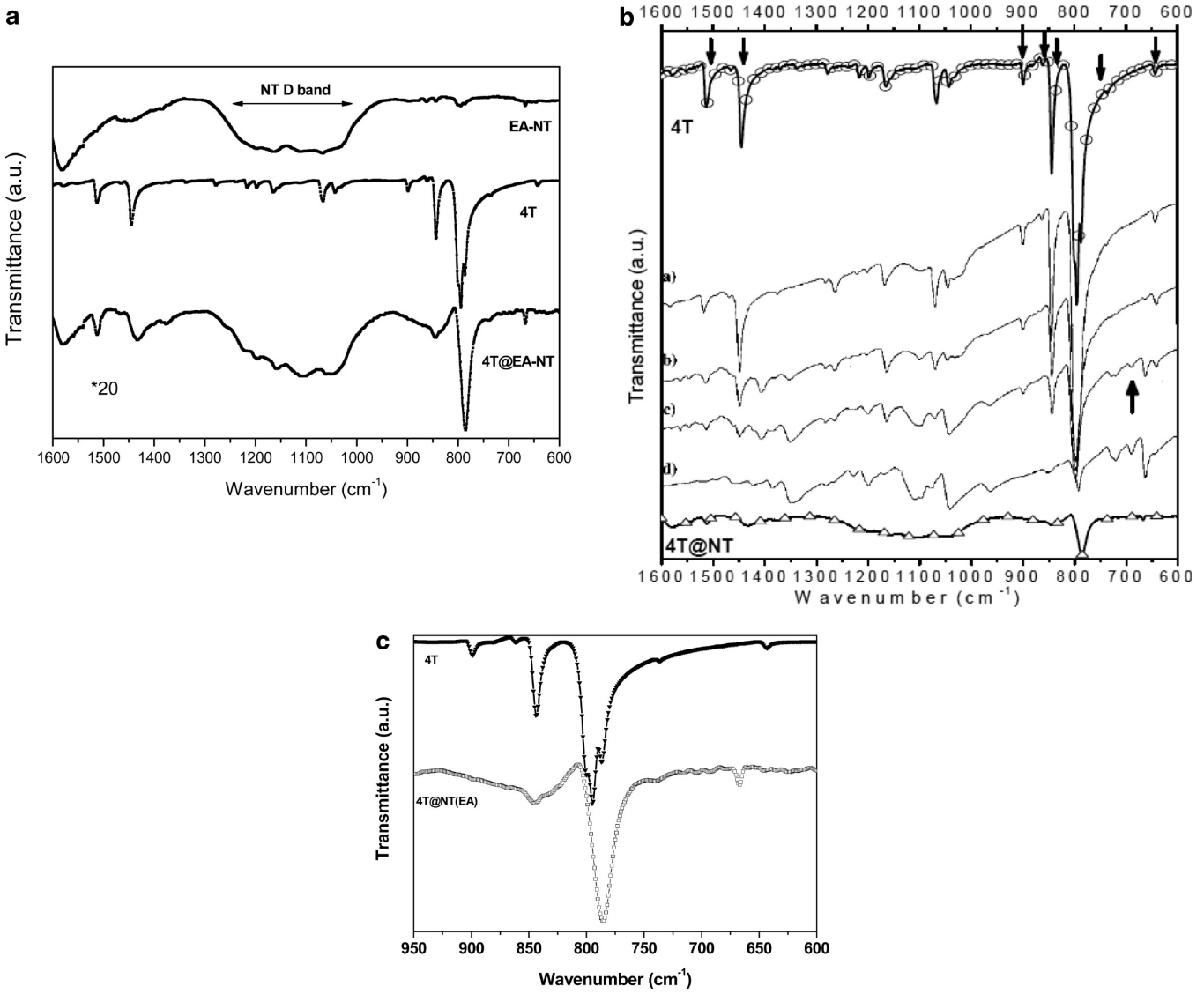

Figure 5. (a) Infrared spectra of pristine EA-NT (top curve), pristine 4T (middle curve), and 4T @NT (bottom curve). The spectra are vertically translated for clarity, and the intensity of the 4T@NT spectrum is multiplied by 20. (b) Infrared transmittance spectra of raw 4T (open circles, top) and 4T inserted NTs (triangles, bottom) together with iodine-doped 4T (gray lines) from ref 39 (spectra a, b, c, d correspond respectively to pristine (a) and time doping (td) of 7, 30 min and td > 1 h), with the kind authorization of Prof. Juan T. López Navarrete. The spectra are vertically translated for clarity. Arrows indicate the IR peaks of 4T mainly affected by the encapsulation process. (c) Infrared spectra of raw 4T (full triangles) and 4T@NT (open squares). The spectra are vertically translated for clarity.

Figure 7a displays the Raman spectra of raw (bottom curves) and 4T@NT (top curves) for the CVD-NT samples at two different excitation wavelengths (488 and 514.5 nm). The 4T encapsulation clearly gives rise to an important loss of the RBM intensities and to a slight downshift of the G-band. If both behaviors are consistent with a charge transfer,[17,18,25,26] the G-band downshift can only be explained by a negative charge transfer on the nanotubes,[26] in good agreement with IR results which suggest a positive charge transfer on the 4T. However, as reported in the TEM section, the CVD-NT sample contains both single and multiwalled nanotubes, exhibits a quite large diameter distribution (from 1 to 2 nm), and thus contains both semiconducting and metallic nanotubes. Such a mixture could hinder our interpretation. Thus, the Raman studies have been focused on the EA-NT samples in the following.

Figure 7b displays the Raman spectra of raw (bottom curves) and 4T@NT (top curves) for the EA-NT samples at different excitation wavelengths. This sample contains no or negligible amount of MWNT and exhibits a rather narrow diameter distribution (1.44 ± 0.22 nm) according to the analysis of the RBM measured below 300 cm^{-1}. Thus, selecting the excitation wavelength properly allows probing either semiconducting or metallic nanotubes. It turns out that at least two distinct Raman signatures are displayed depending on the excitation wavelength.

Indeed, the Raman responses of 4T@NT for low excitation wavelengths (514.5, 488, and 458 nm) are very similar to those obtained with the CVD-NT since the 4T encapsulation leads to the vanishing of the RBM and to a G-band shift (from 1 to 3 cm^{-1}). In fact, the direction of the shift (up) is unlike the CVD-NT sample (down). This difference can be easily explained by considering the difference in tube diameters. Large diameters

give rise to stronger EPC, so that the renormalization effect is more important than the softening of the modes under negative charge transfer,[26] unlike the small diameter tubes, in good agreement with the Raman data obtained respectively on the EA-NT and the CVD-NT.

For 1064 and 752 nm, the 4T encapsulation mainly gives rise to the following changes: (i) tiny or no modification of the G-band profile, (ii) slight modifications of the RBM profile, and (iii) significant upshift of the RBM (from 3 to 10 cm^{-1}). This latest point is consistent with a filling effect of the nanotubes, leading to a strengthening of the interatomic force constants.[8] The first two points rather indicate a very weak charge transfer between 4T and nanotubes since RBM are expected to vanish and the G-band should shift under charge transfer.[17,18,25] Those results are in good agreement with previous studies on sexithiophene encapsulated into nanotubes.[8,13] However, we mentioned from IR experiments a significant positive charge transfer on the conjugated polymers. In fact, considering here an average tube diameter of 1.35 nm deduced from the RBM frequency, the number of carbon atoms surrounding a 4T molecule (20 nm length) is about 400. We can thus infer that the charge transfer remains weak for the nanotubes, leading to tiny modifications of the EA-NT Raman spectra.

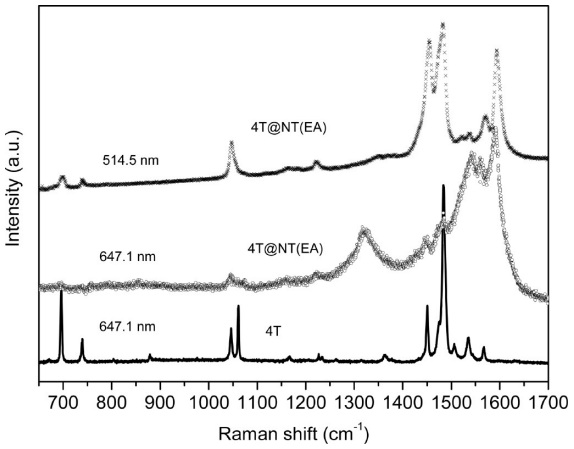

Figure 6. Raman spectra of pristine 4T recorded at an excitation wavelength of 647.1 nm (bottom) and of 4T@NT(EA) recorded at excitation wavelengths of 647.1 nm (middle) and 514.5 nm (top) respectively.

The Raman spectrum recorded with the 647.1 nm excitation wavelength is quite peculiar. Indeed, most of the modifications are similar to those observed at 1064 and 752 nm, but the very important shift (10 cm^{-1}) of the RBM is also observed on the G-band. Furthermore, the 2D band undergoes a shift of about 20 cm^{-1} (not shown), meaning that the modes undergo a rigid upshift, unlike what is observed with the other excitation wavelengths. We have no hypothesis to account for this behavior. Anyway, we assume at 647.1 nm a weak charge transfer, as observed at 1064 and 752 nm.

To summarize, two Raman regimes are displayed as a function of the excitation wavelength. The first one, from 514.5 to 458 nm, gives rise to important modifications that suggest a significant charge transfer between both systems. The second one, from 647.1 to 1064 nm, is consistent with a filling of the nanotubes and a weak charge transfer between 4T and NTs. By the way, the

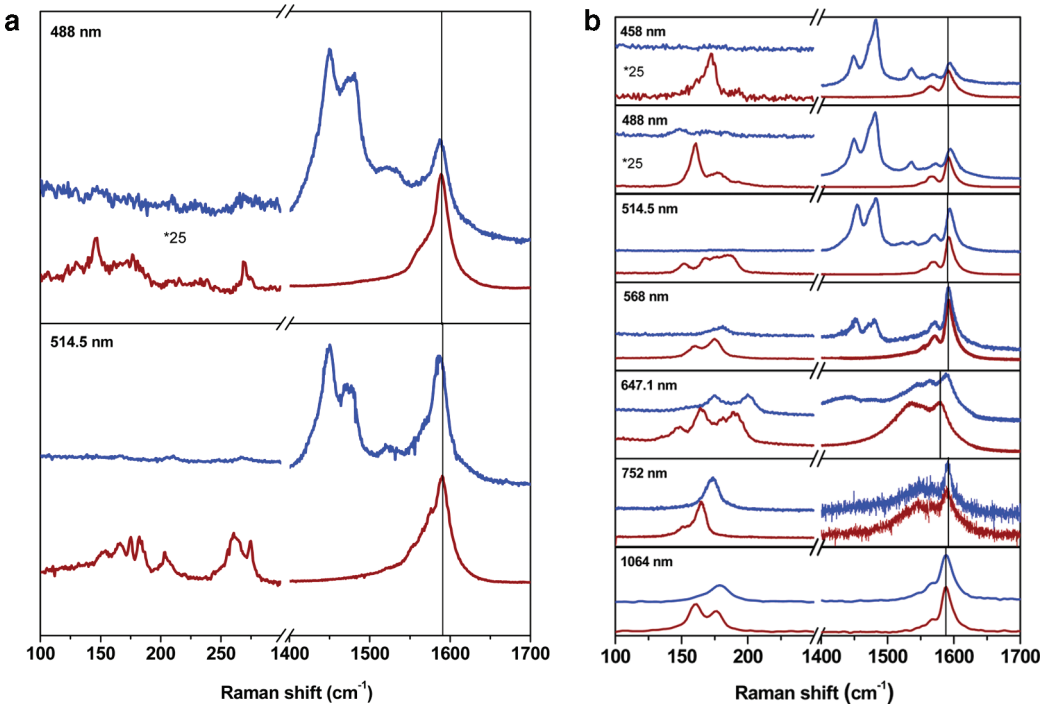

Figure 7. (a) Raman spectra of raw NT (bottom, wine curve) and 4T inserted NTs (top, blue curve) for the CVD-NT sample for two different excitation wavelengths (514.5 and 488 nm). Spectra are normalized on the nanotubes G-band intensity. With 488 nm as excitation wavelength, RBM intensity of both pristine CVD-NT and 4T@EA-NT has been multiplied by 25 for clarity. (b) Raman spectra of raw NT (bottom, wine curve) and 4T inserted NTs (top, blue curve) for the EA-NT for different excitation wavelengths. Spectra are normalized on the nanotubes G-band intensity. The spectrum of the G-band at 752 nm is noisy because of the CCD cutoff. With 458 and 488 nm as excitation wavelengths, RBM intensity of both EA-NT and 4T@EA-NT has been multiplied by 25 for clarity.

spectrum recorded at 568 nm displays an intermediate behavior, with no shift of the G-band, a significant shift of the RBM, and an important loss of the RBM intensity. Furthermore, decreasing the excitation wavelength obviously leads to an important enhancement of the 4T Raman signal (in the 1400−1500 cm^{-1} range) with respect to the nanotubes G-band. The 4T Raman modes intensity certainly increases because the excitation energy is getting closer to the 4T optical absorption energy (close to 400 nm or 3 eV). We thus claim that increasing the excitation energy gives rise to a photoinduced charge transfer between nanotubes and the oligomer. Consequently, the two Raman regimes could actually correspond to in and out of resonance of the 4T molecules.

CONCLUSION

Confinement of dimethyl-quaterthiophene into carbon nanotubes was investigated using HR-TEM, SR-EELS, IR, and Raman spectroscopies. From SR-EELS we detected sulfur inside NTs. Both Raman and IR spectroscopy have provided valuable information about the interaction between the 4T molecules and nanotubes. IR spectra of the 4T@NT exhibits many similarities with those of iodine-doped 4T, suggesting a significant positive charge transfer of the oligomers trapped into nanotubes. Furthermore, a detailed analysis of the Raman G-band before and after the oligomer insertion inside nanotubes states a negative charge transfer of the nanotubes. However, Raman spectra suggest that nanotubes, independent of their metallic or semiconducting character, are only slightly affected by this charge transfer when the excitation energy of the laser is far away from the 4T optical absorption energy. By contrast, a significant charge transfer has been evidenced when the excitation energy is getting close to this absorption energy and assigned to a photoinduced charge transfer. Experiments are in progress to light the photoinduced process.

ACKNOWLEDGMENT

The EELS measurements have been developed at the STEM group of the Laboratoire de Physique des Solides (LPS) at the University of Paris-Sud (Orsay—France). We acknowledge this group for their support and especially Odile Stephan for fruitful discussions.

The authors thank Prof. Juan T. López Navarrete for his kind authorization of utilizing his data on iodine-doped dimethyl-quaterthiophene.

REFERENCES

(1) Berson, S.; Cecioni, S.; Billon, M.; Kervella, Y.; de Bettignies, R.; Bailly, S.; Guillerez, S. *Sol. Energy Mater. Sol. Cells* **2010**, *94*, 699–708.
(2) Videlot-Ackermann, C.; Zhang, J.; Ackermann, J.; Brisset, H.; Didane, Y.; Raynal, P.; El Kassmi, A.; Fages, F. *Curr. Appl. Phys.* **2009**, *9*, 26–33.
(3) Clarke, T. M.; Gordon, K. C.; Chan, W. S.; Phillips, D. L.; Wagner, P.; Officer, D. L. *ChemPhysChem* **2006**, *7*, 1276–1285.
(4) Park, J. H.; Kim, J. S.; Lee, J. H.; Lee, W. H.; Cho, K. *J. Phys. Chem. C* **2009**, *113*, 17579–17584.
(5) Stylianakis, M. M.; Mikroyannidis, J. A.; Kymakis, E. *Sol. Energy Mater. Sol. Cells* **2010**, *94*, 267–274.
(6) El Amrani, A. Ph.D Thesis, University of Limoges, 2008.
(7) Lucas, B.; El Amrani, A.; Chakaroun, M.; Ratier, B.; Antony, R.; Moliton, A. *Thin Solid Films* **2009**, *517*, 6280–6282.
(8) Loi, M. A.; Gao, J.; Cordella, F.; Blondeau, P.; Menna, E.; Bartova, B.; Hebert, C.; Lazar, S.; Botton, G. A.; Milko, M.; Ambrosch-Draxl, C. *Adv. Mater.* **2010**, *22*, 1635–1639.
(9) Babaa, M. R.; Bantignies, J. L.; Alvarez, L.; Parent, P.; Le Normand, F.; Gulas, M.; Mane, J. M.; Poncharal, P.; Doyle, B. P. *J. Nanosci. Nanotechnol.* **2007**, *7*, 3463–3467.
(10) Song, M.; Wang, X. M.; Liu, W.; Zuo, J. L. *J. Colloid Interface Sci.* **2010**, *343*, 48–51.
(11) Roquelet, C.; Lauret, J. S.; Alain-Rizzo, V.; Voisin, C.; Fleurier, R.; Delarue, M.; Garrot, D.; Loiseau, A.; Roussignol, P.; Delaire, J. A.; Deleporte, E. *ChemPhysChem* **2010**, *11*, 1667–1672.
(12) Malard, L. M.; Nishide, D.; Dias, L. G.; Capaz, R. B.; Gomes, A. P.; Jorio, A.; Achete, C. A.; Saito, R.; Achiba, Y.; Shinohara, H.; Pimenta, M. A. *Phys. Rev. B* **2007**, *76*, 233412.
(13) Kalbac, M.; Kavan, L.; Gorantla, S.; Gemming, T.; Dunsch, L. *Chem.—Eur. J.* **2010**, *16*, 11753–11759.
(14) Dresselhaus, M. S.; Dresselhaus, G.; Saito, R.; Jorio, A. *Phys. Rep.* **2005**, *409*, 47–99.
(15) Thomsen, C.; Reich, S.; Maultzsch, J. *Philos. Trans. R. Soc. A* **2004**, *362*, 2337–2359.
(16) Araujo, P. T.; Pesce, P. B. C.; Dresselhaus, M. S.; Sato, K.; Saito, R.; Jorio, A. *Physica E* **2010**, *42*, 1251–1261.
(17) Harley, E. C. T.; McNeil, L. E. *J. Phys. Chem. Solids* **2004**, *65*, 1711–1718.
(18) Chen, G.; Furtado, C. A.; Kim, U. J.; Eklund, P. C. *Phys. Rev. B* **2005**, *72*, 155406.
(19) Jorio, A.; Saito, R.; Dresselhaus, G.; Dresselhaus, M. S. *Philos. Trans. R. Soc. A* **2004**, *362*, 2311–2336.
(20) Kataura, H.; Kumazawa, Y.; Maniwa, Y.; Umezu, I.; Suzuki, S.; Ohtsuka, Y.; Achiba, Y. *Synth. Met.* **1999**, *103*, 2555–2558.
(21) Jorio, A.; Souza, A. G.; Dresselhaus, G.; Dresselhaus, M. S.; Swan, A. K.; Unlu, M. S.; Goldberg, B. B.; Pimenta, M. A.; Hafner, J. H.; Lieber, C. M.; Saito, R. *Phys. Rev. B* **2002**, *65*, 155412.
(22) Piscanec, S.; Lazzeri, M.; Mauri, F.; Ferrari, A. C.; Robertson, J. *Phys. Rev. Lett.* **2004**, *93*, 185503.
(23) Lazzeri, M.; Piscanec, S.; Mauri, F.; Ferrari, A. C.; Robertson, J. *Phys. Rev. B* **2006**, *73*, 155426.
(24) Das, A.; Sood, A. K.; Govindaraj, A.; Saitta, A. M.; Lazzeri, M.; Mauri, F.; Rao, C. N. R. *Phys. Rev. Lett.* **2007**, *99*, 136803.
(25) Tsang, J. C.; Freitag, M.; Perebeinos, V.; Liu, J.; Avouris, P. *Nat. Nanotechnol.* **2007**, *2*, 725–730.
(26) Kalbac, M.; Farhat, H.; Kavan, L.; Kong, J.; Dresselhaus, M. S. *Nano Lett.* **2008**, *8*, 3532–3537.
(27) www.nanocarblab.com.
(28) www.cheaptubes.com.
(29) Takenobu, T.; Takano, T.; Shiraishi, M.; Murakami, Y.; Ata, M.; Kataura, H.; Achiba, Y.; Iwasa, Y. *Nat. Mater.* **2003**, *2*, 683–688.
(30) Jeanguillaume, C.; Colliex, C. *Ultramicroscopy* **1989**, *28*, 252–257.
(31) Arenal, R.; de la Pena, F.; Stephan, O.; Walls, M.; Tence, M.; Loiseau, A.; Colliex, C. *Ultramicroscopy* **2008**, *109*, 32–38.
(32) Lin, H.; Arenal, R.; Enouz-Vedrenne, S.; Stephan, O.; Loiseau, A. *J. Phys. Chem. C* **2009**, *113*, 9509–9511.
(33) Arenal, R.; Stephan, O.; Bruno, P.; Gruen, D. M. *Appl. Phys. Lett.* **2009**, *94*, 111905.
(34) Ayala, P.; Arenal, R.; Rummeli, M.; Rubio, A.; Pichler, T. *Carbon* **2010**, *48*, 575–586.
(35) Bachilo, S. M.; Strano, M. S.; Kittrell, C.; Hauge, R. H.; Smalley, R. E.; Weisman, R. B. *Science* **2002**, *298*, 2361–2366.
(36) Li, L. J.; Khlobystov, A. N.; Wiltshire, J. G.; Briggs, G. A. D.; Nicholas, R. J. *Nat. Mater.* **2005**, *4*, 481–485.
(37) Yanagi, K.; Iakoubovskii, K.; Matsui, H.; Matsuzaki, H.; Okamoto, H.; Miyata, Y.; Maniwa, Y.; Kazaoui, S.; Minami, N.; Kataura, H. *J. Am. Chem. Soc.* **2007**, *129*, 4992–4997.
(38) Bantignies, J. L.; Sauvajol, J. L.; Rahmani, A.; Flahaut, E. *Phys. Rev. B* **2006**, *74*, 195424.
(39) Sbai, K.; Rahmani, A.; Chadli, H.; Bantignies, J. L.; Hermet, P.; Sauvajol, J. L. *J. Phys. Chem. B* **2006**, *110*, 12388–12393.

(40) Hernandez, V.; Casado, J.; Ramirez, F. J.; Zotti, G.; Hotta, S.; Navarrete, J. T. L. *J. Chem. Phys.* **1996**, *104*, 9271–9282.
(41) Casado, J.; Hernandez, V.; Hotta, S.; Navarrete, J. T. L. *J. Chem. Phys.* **1998**, *109*, 10419–10429.
(42) Casado, J.; Bengoechea, M.; Navarrete, J. T. L.; Otero, T. F. *Synth. Met.* **1998**, *95*, 93–100.